Super-Resolution Methods for Wideband Radar

Sidney L. Borison, Stephen B. Bowling, and Kevin M. Cuomo

Lincoln Laboratory has investigated two concepts for improving the resolution of wideband coherent radar data. The first concept uses modern spectral-analysis methods for improving resolution relative to the restrictions of conventional Fourier processing. These spectral methods extrapolate signals in a radar frequency dimension by a process called bandwidth extrapolation (BWE). The methods can also be used for signals collected over limited time intervals. The second concept uses image signal processing models that correspond to rotating point motion. The models allow extended coherent processing (ECP) over wider target rotation angles, resulting in improved Doppler (cross-range) resolution. For sufficiently large rotation angles and for constant-amplitude scattering centers, ECP also improves the range resolution.

This article discusses BWE and ECP theory and methods, and presents examples from simulations and model measurement data. Also included is a discussion of the expected precision of BWE-enhanced resolution and its dependence on the signal-to-noise ratio.

Resolution is a controlling factor in estimating details of a target's structure from processed wideband coherent radar data. Typical analyses require the examination of radar signal responses in one and two dimensions of target extent, usually displayed in range-time-intensity (RTI), Doppler-time-intensity (DTI), and range-Doppler-intensity image plots. Most targets are rigid, isolated objects with relative rotations that allow the Doppler return to be related to a cross-range dimension along an axis that is orthogonal to the slant range, i.e., the range along the radar line of sight (RLOS). Fourier integration relations in conventional processing define resolution in these dimensions to be inversely proportional to the total integration intervals: transmitted bandwidth for slant range and allowable relative rotation angle for cross-range. To enable simplifications of the range-Doppler processing, the motion of the rotating target points that are positioned away from the effective rotation center must be small relative to the expected resolution.

Classical range resolution ΔR_c is inversely proportional to bandwidth. With sidelobe suppression, it can be expressed as

$$\Delta R_c = 1.8 \frac{c}{2W}, \qquad (1)$$

where c is the propagation speed and W is the signal bandwidth. The value of ΔR_c defined above is the –6-dB width of the individual point response function. A plot of classical range resolution as a function of signal bandwidth appears in Figure 1. The figure also illustrates a common signal implementation in which a linear frequency modulated (LFM) pulse is transmitted and the reflected signal is received through a matched filter. Thus, for example, a 1-GHz bandwidth provides a 27-cm range resolution. Hardware modifications and developments to increase the signal bandwidth are expensive, and there are often technology limitations, e.g., wideband high-power tubes. For additional radar and signal details, see, for example, Reference 1.

Classical cross-range resolution ΔXR_c is inversely proportional to rotation angle $\Delta\theta$ and directly pro-

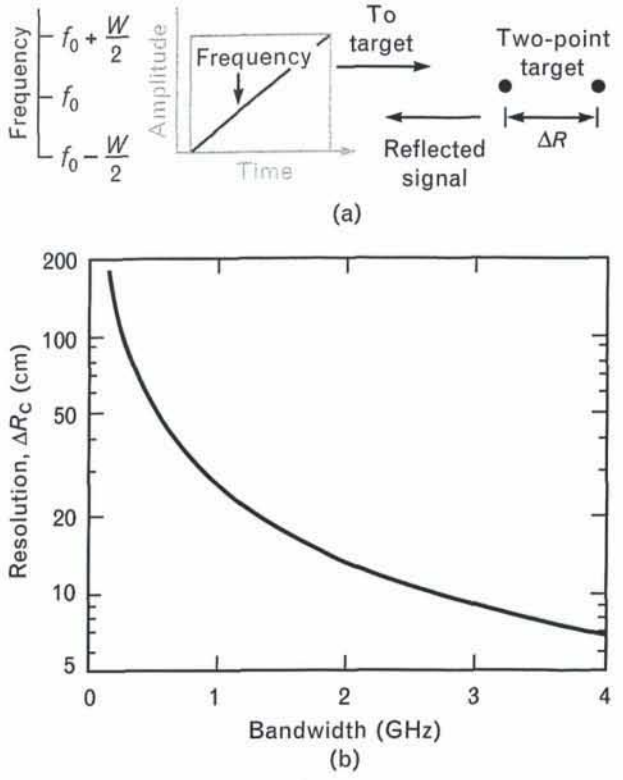

FIGURE 1. Classical range resolution as a function of signal bandwidth: (a) transmitted waveform and (b) resolution obtained with matched-filter receiver including sidelobe suppression.

portional to radar wavelength λ. With sidelobe suppression, it can be expressed as

$$\Delta XR_c = 1.8 \frac{\lambda}{2\Delta\theta}.$$

For a stationary radar tracking a rotating target, $\Delta\theta = \omega T$, where ω is the angular rotation rate and T is the duration of the Doppler-processed time series. This application of Doppler resolution is called Inverse Synthetic-Aperture Radar (ISAR). For a stationary target observed by a moving radar, the effective angular rotation rate is $\omega = V/R$, where V is the velocity of the radar and R is the distance to the target. This application of Doppler resolution is called Synthetic-Aperture Radar (SAR), and the product VT is called the synthetic aperture. For additional details, see, for example, References 2 and 3. For either ISAR or SAR processing, the data interval is generally selected to obtain a cross-range resolution comparable to the slant-range resolution.

Lincoln Laboratory has recently investigated two concepts for potential resolution improvement. The first concept uses modern spectral-analysis methods to improve the slant-range resolution relative to the restrictions of conventional Fourier processing. These spectral methods extrapolate signals in a radar frequency dimension by a process called bandwidth extrapolation (BWE). Figure 2 illustrates the practical steps typically used in BWE, with the input measurement data in the form of signal amplitude and phase versus slant range. To illustrate the potential of this technique, examples of processed data from model range measurements of two small spheres, 10 cm apart, are shown. The input pulse does not resolve the spheres because the 1-GHz bandwidth limits the resolution to about 27 cm. A radar frequency-domain representation of the input signal is obtained with the transforms indicated. A least-squares estimation method calculates the linear-prediction coefficients from the spectral data, and the coefficients are used to extrapolate the data to produce signals with a spectrum of 4-GHz bandwidth. The resulting pulse response based on the extrapolations clearly shows two peaks. Also shown in the figure is the pulse response for the true 4-GHz measurement data. Note how close the two curves are. Details of the methods and measurement results of Figure 2 are discussed further in the following section.

The second concept investigated at Lincoln Laboratory improves the Doppler, or cross-range, resolution. When the data collection includes a large target rotation angle (i.e., the *spotlight* mode for either ISAR or SAR), the use of image signal processing models that account for the motion of rotating points can improve the cross-range resolution. This technique removes range- and Doppler-walk restrictions and allows extended coherent processing (ECP) over wider target rotation angles, as shown in Figure 3. The figure illustrates an approximate method for obtaining an ECP image of a wider integration angle by coherently summing responses from a set of range-Doppler images of narrower integration angles. Also shown are theoretical responses from an array of nine equal-amplitude points, which show that range-Doppler responses for the wider integration increasingly smear with distance from the rotation center.

ECP, on the other hand, produces uniform responses that preserve the two-dimensional resolution. The use of BWE to improve the slant-range resolution further restricts the range-Doppler integration. In such cases, ECP may be required to preserve the improved resolution. Further details of ECP are presented in the section "Extended Coherent Processing."

When the data collection does not include a large target rotation angle (i.e., short data intervals for ISAR or the *strip mapping* mode for SAR), the use of modern spectral methods can be applied in two dimensions. One-dimensional super-resolution is first applied to extrapolate the data in time (angle) for each slant-range sample. Conventional processing is then used to obtain the improved cross-range resolution, after which super-resolution is applied to each cross-range (Doppler) gate to improve the range resolution.

Figure 4 contains a conventional image that was obtained with data simulated for a cone model represented by three point-scatterers. The signal bandwidth and angular-rotation interval are inadequate to resolve the three image points. Figure 4 also shows the results obtained by applying sequential super-resolution as described in the preceding paragraph with data expansion in each dimension by a factor of 3. Additional discussion of this process is presented in the subsection "Simulated 2-D Super-Resolution Using Sequential 1-D Super-Resolution."

The sequential application of a one-dimensional algorithm can produce results that differ depending on the order of processing, i.e., time expansion, then bandwidth extrapolation, or vice versa. Furthermore, sequential processing may not obtain the optimum results when it is compared to a two-dimensional (or multidimensional) algorithm, e.g., the maximum likelihood method, or minimum variance, discussed in References 4 through 6.

Bandwidth-Extrapolation Methods

In the late 1960s, R.T. Lacoss began investigating the application of super-resolution techniques to seismic

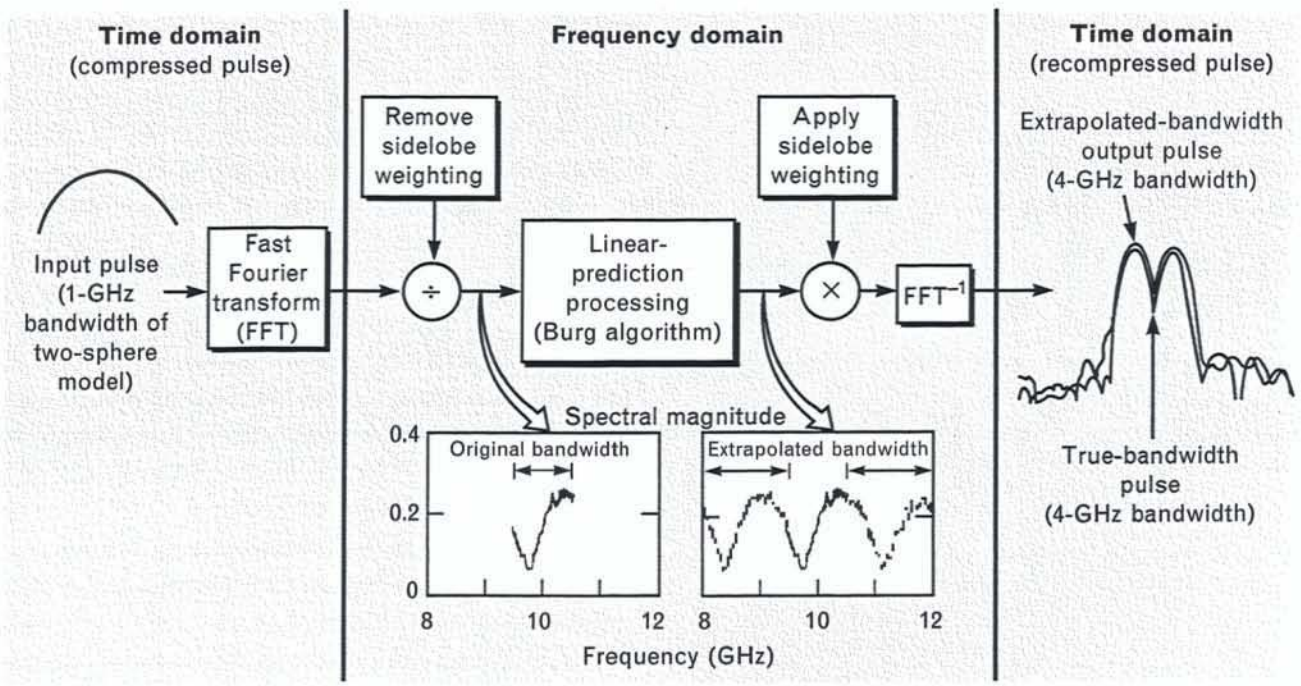

FIGURE 2. Bandwidth extrapolation (BWE) process for improved range resolution. The examples of processed data are from X-band model range measurements of two small spheres, 10 cm apart. The input pulse shown on the left does not resolve the spheres because the 1-GHz bandwidth limits the resolution to about 27 cm. A least-squares estimation method calculates the linear-prediction coefficients from the spectral data, and the coefficients are used to extrapolate the data to produce signals with a spectrum of 4-GHz bandwidth. In the resulting pulse response shown on the right, two peaks are clearly visible. Also shown on the right is the pulse response for the true 4-GHz measurement data.

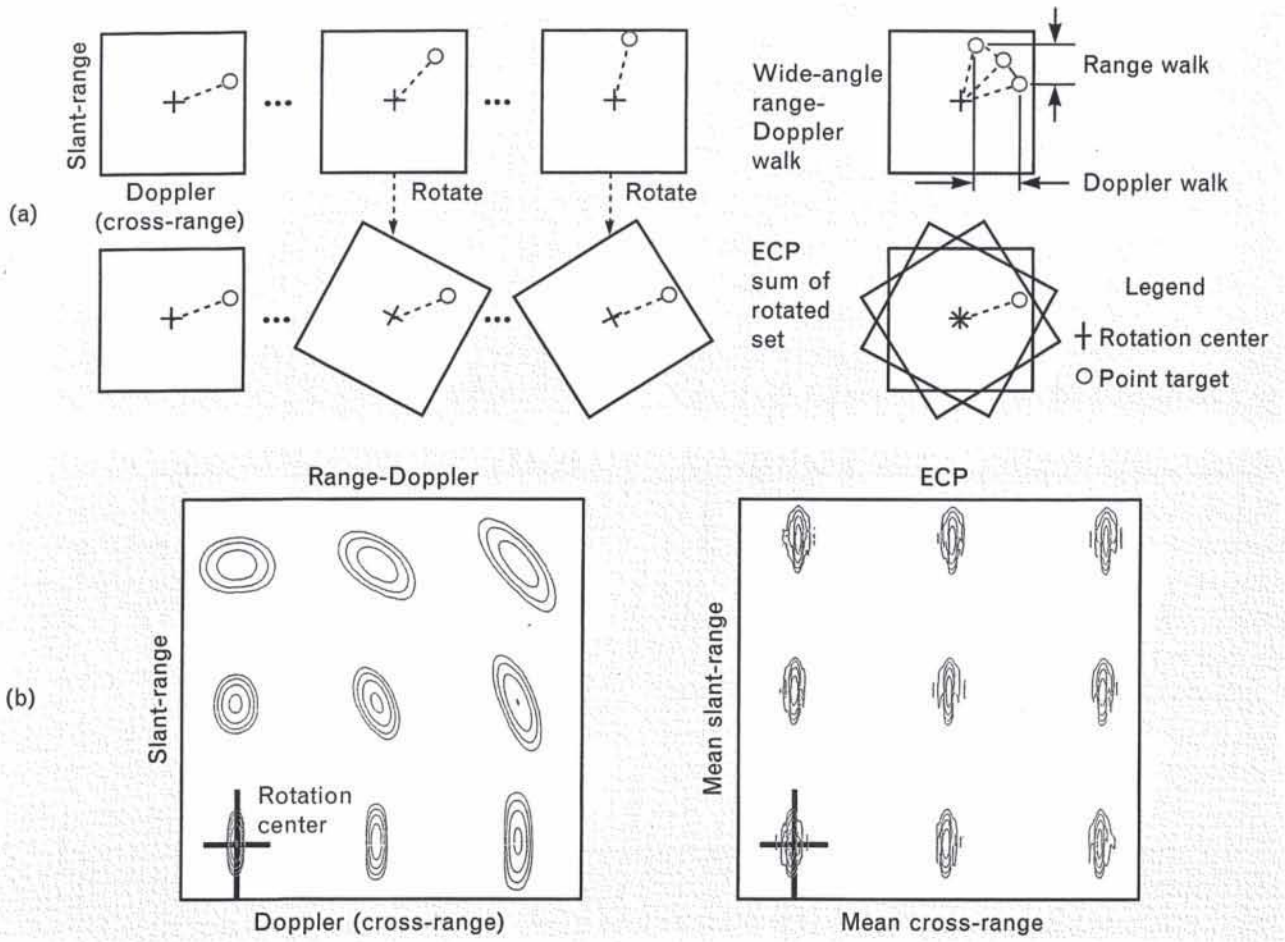

FIGURE 3. Extended coherent processing (ECP) technique: (a) an approximate method for obtaining an ECP image of a wider integration angle by coherently summing responses from a set of range-Doppler images of narrower integration angles, and (b) examples of simulated point-model responses from an array of nine equal-amplitude points spaced 1 m in the horizontal and vertical directions (the contours represent 5-dB intervals). The data were obtained with a 1-GHz bandwidth at X band and a rotation angle of 20°. Note that ECP produces uniform responses that preserve the two-dimensional resolution.

discrimination [4]. Starting in the late 1970s, these techniques were applied to super-resolution angle-of-arrival estimates [7]. The application of the Burg method for Doppler-processing enhancement was explored by S.B. Bowling in 1977 [8], when he also mentioned the potential for improving range resolution. In 1990, K.M. Cuomo investigated the Burg method for extrapolating signals in the radar frequency dimension as a means of improving the range resolution of coherent radar returns [9]. These proposed methods use the estimated parameters to extrapolate data, thus preserving the amplitude and phase. These data could then be Fourier processed to obtain the improved resolution responses. Preservation of the phase is essential in range-Doppler image processing. Cuomo applied this technique to field data and achieved remarkable results, leading to the current interest in these methods.

In the first-order far-field backscatter modeling of radar signals, all reflections are assumed to be from discrete points with complex scattering coefficients (amplitude and phase) that are constant with incident radar frequency. The only variation with frequency is a phase term that is linearly proportional to the range time delay, equal to $2r/c$, where r is the slant range and c is the speed of light. The total response from such a target is modeled as the sum of complex sinusoids, with radar frequency as the independent vari-

able and the frequencies of the sinusoids determined by the range time delay. A Fourier transform of signals in a band of radar frequencies then produces a pulsed response in range time delay in which the peaks in the pulses correspond to point locations. The pulsed response also indicates the scattering coefficient amplitudes and phases. Note that this terminology is the converse of, but equivalent to, more frequently encountered time-series analyses in which continuous sinusoids in time transform to pulses in frequency.

First-order point-response modeling is expected to be a realistic approximation for most of the direct-ray effects that are anticipated for practical targets many wavelengths in extent. Direct-ray discrete reflections are expected to vary only slightly with radar frequency across a typical signal bandwidth. Responses from multipath rays between points and surfaces can generally be treated as sinusoids that include the total-path range time delays. Resonant scattering within the observation band would be a significant deviation but is rarely expected.

Conventional Fourier processing of the signal from a single point produces a pulse function with a mainlobe width in range that is inversely proportional to the radar frequency bandwidth of the integration. Sidelobe-reduction weighting is usually included and increases the mainlobe spread. For multiple point-scatterers, the Fourier transform response in range time delay is the linear sum of individual point responses; resolution of the points is limited by the –6-dB width of the individual point response function. Thus the conventionally processed signal is limited in point range resolution by the radar frequency bandwidth. This Fourier process can be viewed as a correlation integral of the total signal with respect to a one-sinusoid reference, requiring only a one-parameter search but making the resolution of multiple points dependent on the spread in a one-point response function.

Correlation with a multiple-sinusoid model could

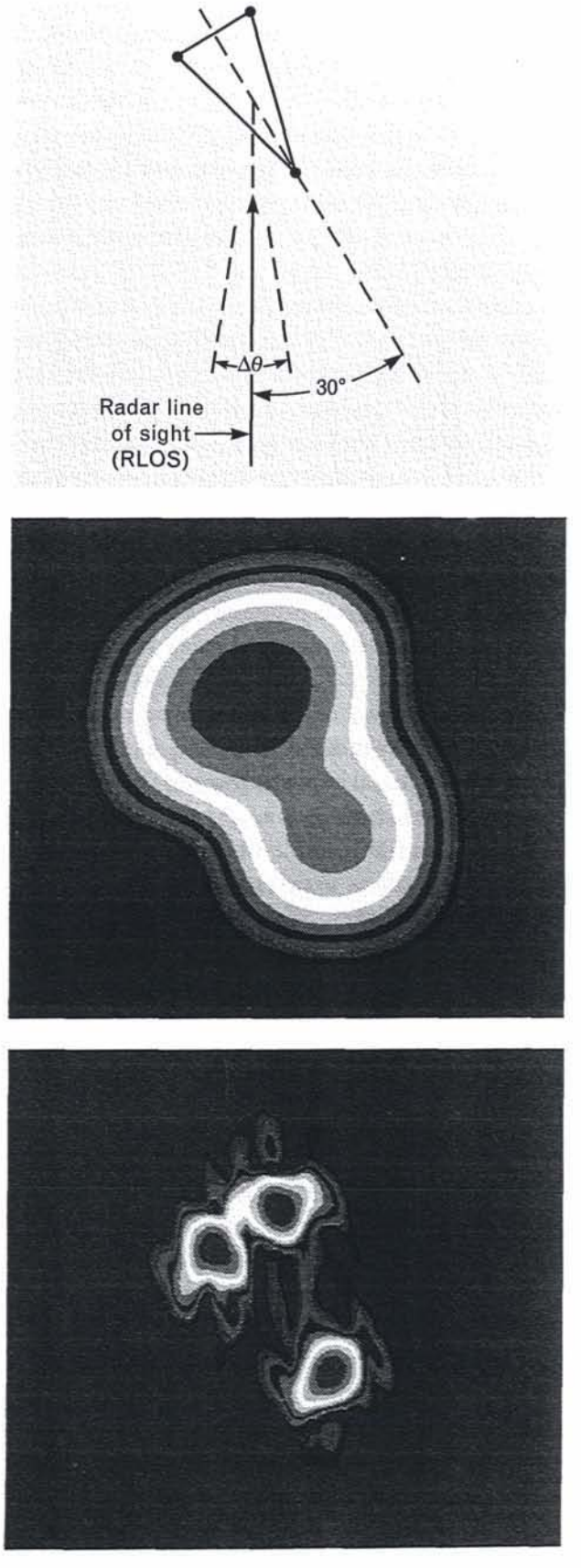

FIGURE 4. Example of two-dimensional super-resolution using sequential one-dimensional super-resolution: (top) diagram of three-point cone model and geometry used, (middle) conventional image of model, and (bottom) super-resolution image of model.

obtain better resolution but is not considered practical due to the increase in data processing required. As an alternative to correlation processing, a data-fitting process, such as nonlinear least squares, might be used to obtain the sinusoid parameter set that gives a good match between theoretical signal data and experimental measurements. On this basis, if at least a minimal data set (relative to the number of unknown parameters) is available and no errors perturb these data, the separation of frequencies of two sinusoids can be estimated independent of the length of the total data interval. As noise perturbations appear, however, the parameter estimates will increase in error with shorter data interval and may become meaningless, especially because of the nonlinearity in the modeling. Furthermore, if the true number of sinusoids is unknown, the modeling is not fully constrained, allowing additional instability in the estimates.

Such direct nonlinear parameter estimation is considered impractical for most real radar data problems. To gain computational practicality, most super-resolution spectral methods do not constrain the signal model to pure undamped sinusoids, so the estimations are not optimal in the fully constrained sense. In super-resolution methods, the characterization of responses is based on parametric modeling, which allows coupling effects between the signals and noise. Determination of these effects generally requires numerical investigation for particular conditions.

A linear-prediction signal model appears to be the most practical constraint on measurement data in general spectral-analysis problems. The model assumes that the sum of an equispaced set of signal samples multiplied by a set of complex weights, or prediction coefficients, will predict the next sample. Furthermore, this set of constant weights can be moved ahead to continue the predictions, i.e., to extrapolate the original data in a forward direction. Complex conjugates of these weights can be used to extrapolate signals in a backward direction. The set of weights is estimated by applying linear least-squares methods to a summation of the squared residuals between the predicted values and the actual measurements.

The linear-prediction coefficients do not contain sinusoid amplitude and phase information directly. With the prediction coefficients, extrapolation of data beyond a measured set can be carried out to a desired limit for subsequent Fourier transformation. But the extrapolation may fail to correspond exactly with that of a simple, undamped sinusoid sum because of deviations that are allowed by the linear-prediction model, which is less constrained than the sum-of-sinusoids model. Nevertheless, the estimations are manageable with more practical methods.

In more general modern spectral-analysis papers, the linear-prediction concept is often used to estimate the coefficients of an autoregressive (AR) model. Generally, the power spectral density (PSD) is estimated as a function of the coefficients alone, without resorting to the extrapolation of signals. The PSD form, which gives a spiky function without ringing sidelobes, may be useful if interest is primarily in the line locations of spectra (i.e., the slant range of points in the radar problem). For Gaussian random processes, the AR PSD is also a maximum entropy estimate, and use of the PSD is sometimes called a maximum entropy method (MEM) or maximum entropy spectral analysis (MESA). For radar applications that require coherent data for subsequent Doppler analysis, the PSD is not of significant value.

The methods of processing vary according to how the linear-prediction coefficients are estimated. Three methods, all based on a forward- and backward-prediction error minimization, have been chosen as potentially practical for radar data-analysis problems: the Burg method, a Marple modified covariance method (which may be viewed as a less constrained version of the Burg method), and a Tufts-Kumaresan method that allows a noise-reduction process within the basic estimator represented in the Marple method.

Linear-Prediction-Coefficient Estimators

Linear-prediction coefficients for extrapolating point-scatterer frequency data can be estimated from a set of measurement data by selecting coefficients to minimize the error between the predicted signal values and the measured values. The Burg, Marple-modified-covariance, and Tufts-Kumaresan methods of spectral analysis can be viewed as starting with similar statements of a linear least-squares estimation problem. Each method considers the sum of the square error of residuals between the actual measurement data and

the backward- and forward-predicted data, and minimizes this total error relative to the predictor coefficients. Thus the forward-prediction error is given by

$$E_n^{\mathrm{f}} = \left| S_n - \hat{S}_n^{\mathrm{f}} \right|^2 \qquad \text{for } n = p+1, \ldots, N,$$

where the forward-prediction filter operation is

$$\hat{S}_n^{\mathrm{f}} = -\sum_{i=1}^{p} a_i S_{n-i},$$

and the backward-prediction error is given by

$$E_n^{\mathrm{b}} = \left| S_n - \hat{S}_n^{\mathrm{b}} \right|^2 \qquad \text{for } n = 1, \ldots, N-p,$$

where the backward-prediction filter operation is

$$\hat{S}_n^{\mathrm{b}} = -\sum_{i=1}^{p} a_i^* S_{n+i}.$$

In the above equations, S_n is the nth frequency sample, $\hat{S}_n^{\mathrm{f}}$ is the estimate of S_n using forward prediction, $\hat{S}_n^{\mathrm{b}}$ is the estimate of S_n using backward prediction, p is the order of the prediction filter, a_i is the ith predictor coefficient, a_i^* is the complex conjugate of the ith predictor coefficient, and N is the total number of data (frequency) samples.

The total prediction error to be minimized relative to the set of a_i is given by

$$E = \sum_{n=p+1}^{N} \left| \sum_{i=0}^{p} a_i S_{n-i} \right|^2 + \sum_{n=1}^{N-p} \left| \sum_{i=0}^{p} a_i^* S_{n+i} \right|^2,$$

where $a_0 = 1$.

Other methods [6] such as the autocorrelation, covariance, and variations on Prony's method use prediction errors only in a single direction, and the results tend to give poorer resolution. Each method mentioned solves for predictor coefficients directly in terms of measured data rather than in terms of autocovariance estimates. Spectral-analysis techniques such as the Yule-Walker and Pisarenko harmonic decomposition methods are considered of lesser value in the BWE problem; they require autocovariance estimates of the measured data and can result in non-realistic autocovariance values.

Burg Method. Developed by J. Burg, this method for coefficient estimation adds a further constraint on the coefficients based on a statistical argument for the form of true AR-model functions [6, 8]. The constraint, called the Levinson recursion, allows the unknown coefficients to be obtained from a sequence of least-squares minimizations in which a single parameter is estimated at each step. The Levinson recursion guarantees that extrapolated data cannot exponentially increase in amplitude. There can, however, be exponential damping; in worst cases, this damping may preclude significant resolution improvement. A good strategy for preventing such an effect appears to be the use of a number of prediction coefficients that is significantly greater than the expected number of sinusoids. The upper limit on the number of coefficients calculable is one less than the number of signal samples, although significantly less than this number is usually chosen because output responses may appear too noisy.

Especially relevant in BWE processing are effects that limit two-point resolution even in the no-noise case. These distortions are illustrated in Figure 5, which shows simulated amplitude-range responses from a pair of equal-amplitude points for separation distances that were decreased in 0.5-cm steps. The figure compares the true 9600-MHz-bandwidth responses without extrapolation to the responses based on 1000-MHz-bandwidth data extrapolated to 9600 MHz with the Burg method. At each range separation chosen, a set of calculations was made by varying the relative phase between the points; the plots show a dispersion when this phase difference significantly affects the responses. From Equation 1, the single point-scattering response for a true 9600-MHz bandwidth will have a –6-dB width (for Hamming weighting) of 2.8 cm. At this range separation, two equal-amplitude scattering centers are resolvable (Figure 5[a]); as the separation decreases further, however, the effects of relative phase cause distortions in the ability to measure the separation.

The distortion effects in the Burg result are more complex (Figure 5[b]). Resolution is not possible when the sidelobes reach high levels and the dispersion of responses with different relative phase values becomes

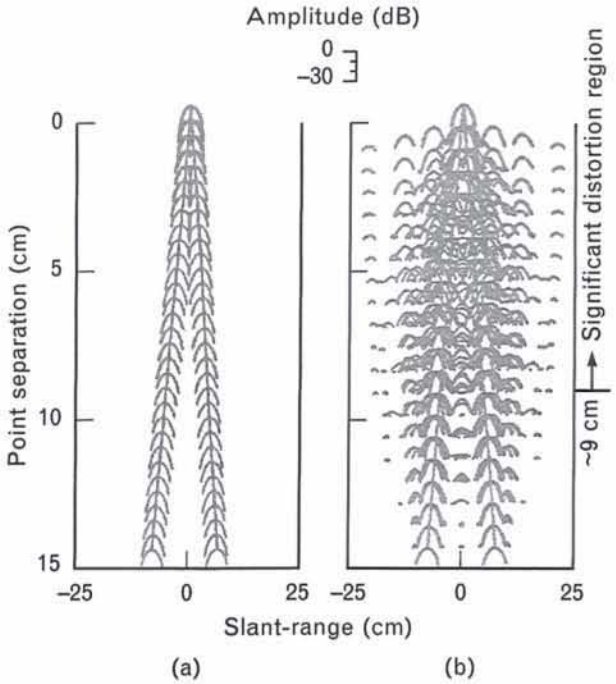

FIGURE 5. Simulated amplitude-range responses from two equal-amplitude points: (a) true 9600-MHz-bandwidth responses without extrapolation and (b) responses from 1000-MHz-bandwidth data extrapolated to 9600 MHz with the Burg method and 26 prediction coefficients. For both plots, there was no noise, the separation distance between the points was decreased in 0.5-cm steps, and a set of calculations was made at each range separation by varying the relative phase between the points in 22.5° steps. From Equation 1, the single point-scattering response for a true 9600-MHz bandwidth will have a –6-dB width (for Hamming weighting) of 2.8 cm. At this range separation, the two points are still resolvable. The distortion effects in the Burg result are more complex. A BWE ratio limit can be estimated as the ratio of the –6-dB point spread of the true bandwidth (i.e., 27 cm for the 1000-MHz bandwidth) to the extrapolated-data resolution limit for tolerable distortions (approximately 9 cm). Thus the BWE ratio limit is approximately 27/9 = 3.

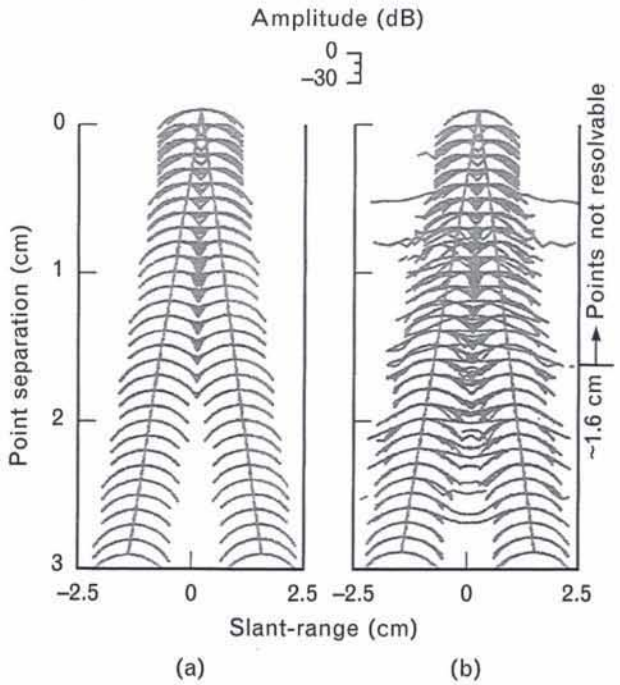

FIGURE 6. Simulated amplitude-range responses from two equal-amplitude points: (a) true 30-GHz responses without extrapolation and (b) responses from 1-GHz-bandwidth data extrapolated to 30 GHz with the Marple method and two prediction coefficients. (The conditions of the experiment are similar to the no-noise conditions of Figure 5, except a separation step of 0.1 cm was used.) A BWE ratio limit can be estimated as the ratio of the –6-dB point spread of the true bandwidth (i.e., 27 cm for the 1-GHz bandwidth) to the extrapolated-data resolution limit for tolerable distortions (approximately 1.6 cm). Thus the BWE ratio limit is approximately 27/1.6 = 17.

great. For the noise-free case, a BWE ratio limit can be estimated as the ratio of the true-bandwidth –6-dB point spread to the extrapolated-data resolution limit for tolerable distortions. As shown in Figure 5, this ratio for the Burg method is estimated as approximately 3:1. The sidelobe structure in Burg responses changes if the number of coefficients is reduced to the minimum of two, but the wide dispersions develop at about the same range separation.

Marple Method. Methods that solve for linear-prediction coefficients by using linear least-squares formulations from residuals based on forward and backward prediction and no other constraints are sometimes referred to as forward-and-backward linear prediction (FBLP). Different investigators have devised FBLP methods in various ways. An FBLP method by S.L. Marple [6], sometimes called the modified covariance method, employs an efficient solution for the resulting linear least-squares normal equations. The Marple method is free of the line-splitting and frequency-bias distortions that are sometimes observed with the Burg method in the real sinusoid problem, but it does not guarantee a stable linear prediction filter. Thus exponential growth of the extrapolated data can occur.

Figure 6 shows the results of a two-point simula-

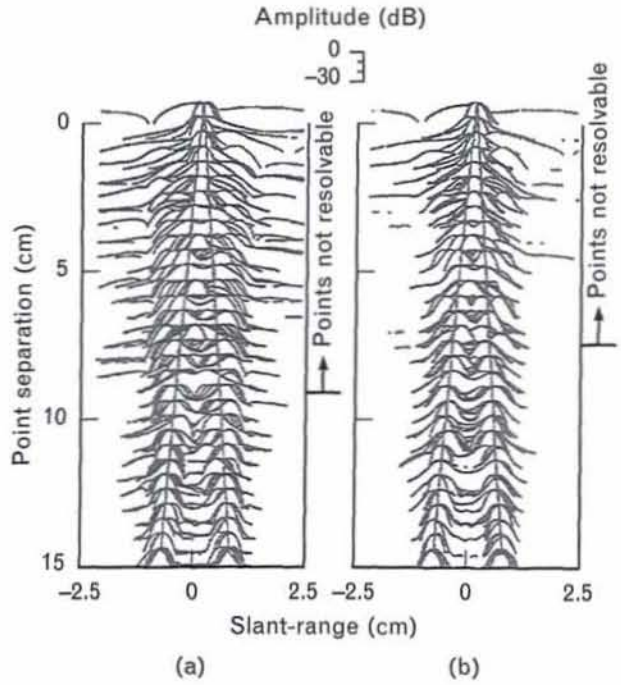

FIGURE 7. Simulated amplitude-range responses for the (a) Burg and (b) Marple BWE methods with noise; the input signal-to-noise ratio was 15 dB (ratio of single peak power to noise power). For both plots, the input bandwidth was 1000 MHz (27 samples), the output bandwidth was 9800 MHz, the separation step was 0.5 cm, the phase was varied in 22.5° steps at each separation, and the number of prediction coefficients used was 10. Note that the Burg results show a resolution limit similar to the no-noise case of Figure 5, while the Marple limit is now only slightly smaller than the Burg limit.

tion with no noise, similar to the simulation of Figure 5, except the data were extrapolated with the Marple method. Note that only two coefficients can be used in the unconstrained FBLP case with no noise. A greater upper limit on the bandwidth extrapolation was used because the Marple result shows almost an order-of-magnitude finer resolution before distortion effects became significant. (Numerical precision may be a factor in this experiment; double precision was used to obtain the results shown.)

FBLP methods, as exemplified in the Marple two-point results, can potentially result in better resolution than the Burg method in conditions of very low noise. FBLP methods, however, are much more sensitive to noise; a reduction to Burg performance in the two-point experiment occurs at noise levels that are generally experienced. Figure 7 shows the results of a two-point simulation that was repeated with noise added for both the Burg and Marple methods. In each case, the noise equivalent power was 15 dB below that of a single point-scatterer signal. The Burg results show a resolution limit similar to the no-noise case of Figure 5; the Marple limit is now only slightly smaller than the Burg limit. Because the FBLP method allows exponential increases in the amplitudes (as opposed to the constraints in the Burg method), catastrophic failure of estimations can result. Such failure tends to depend on the noise condition and on the number of coefficients estimated. Reducing the number of coefficients may remove the exponential growth, but the reduction in coefficients might make the exponential damping too great for any significant improvement in resolution. Such effects have been encountered in BWE simulations with multiple-point models and in experiments with measured data.

Tufts-Kumaresan Noise Reduction. Noise-reduction methods have been suggested to improve the unconstrained FBLP process without the application of a direct constraint on the prediction-coefficient relations such as that applied by Burg. A prominent method that uses eigen-decomposition of the matrices of the normal equations in the unconstrained estimation has been proposed by D.W. Tufts and R. Kumaresan [10, 11]. Their method, also called a modified FBLP, operates on the premise that even though the approximate number of sinusoids may be known, a larger number of prediction coefficients is desirable for better resolution effects. If sinusoid power levels are high enough relative to noise, a singular value decomposition may allow a reconstructed matrix according to an ordering of eigenvalues that omits the terms most probably related to noise. An estimate of the number of sinusoids must be made, either from *a priori* expectations or from a decision based on an eigenvalue comparison. The reconstruction of matrices also provides a smoothed version of the input signal data that can be used with noise-reduced linear-prediction-coefficient estimates for an extrapolated bandwidth data set. This approach is expected to have difficulties in multiple-point cases with widely different reflection amplitudes, even with lower noise levels. In such cases, the sorting based on eigenvalue ordering can lose low-amplitude signal-related terms

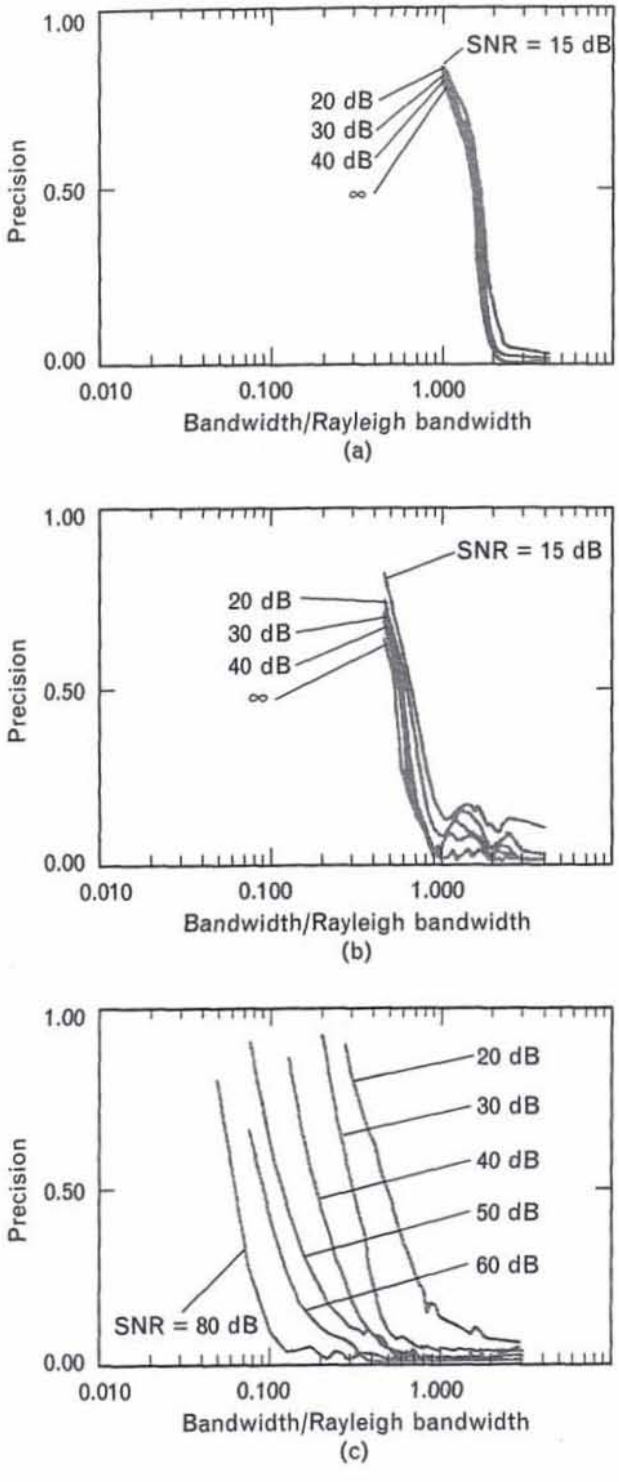

FIGURE 8. Precision versus normalized signal bandwidth for two equal-amplitude points separated by a distance ΔR: (a) no BWE, (b) BWE using the Burg method, and (c) BWE using the Marple method. (Precision is defined as one standard deviation in the separation estimate divided by the true scattering-center separation, i.e., $\sigma_{\Delta R}/\Delta R$.)

and pick up noise-related terms. The results of limited experiments with this method have not been very promising, but conclusions for different conditions not tested have yet to be obtained.

Precision of BWE-Enhanced Resolution

The ability of BWE methods to locate two resolvable peaks that have equal scattering amplitudes have been investigated with simulations. The separation between the peaks was assumed to be that which corresponded to the Rayleigh bandwidth; i.e., $W_R = c/(2\Delta R)$. For the actual signal bandwidth W, a variable, the signal processing for each calculation was adjusted to obtain a constant SNR in the range-profile domain for a resolved point-scatterer. For a given SNR value, Monte Carlo calculations were made at each bandwidth with 100 noise seeds. In addition, the uniform random relative phase between the scattering centers was modeled by calculating a result at 5° steps between 0° and 180°. The precision in estimating the separation is defined as one standard deviation in the estimates divided by the true scattering-center separation; i.e., $\sigma_{\Delta R}/\Delta R$.

Using conventional Fourier processing, Figure 8(a) is a plot of the estimated precision obtained for five different SNR values (∞, 40, 30, 20, and 15 dB) as a function of the normalized signal bandwidth. Clearly, the bandwidth must be sufficiently large to provide good resolution; i.e., approximately 1.8 times the Rayleigh bandwidth (which corresponds to data weighted for sidelobe suppression) is required to obtain a precision of about 0.5. These results will be used below for comparison with estimates that employ bandwidth extrapolation followed by Fourier processing.

Figure 8(b) shows the results when the signal for each bandwidth is first processed by the Burg method with extrapolation by a factor of 10. In each case, this extrapolation factor was well beyond that needed for the required resolution, such that when resolution was possible the two peaks become individually sharper. Note that for a desired value of precision, e.g., 0.5, the required signal bandwidth is about 40% of that required by conventional Fourier processing.

The results of the Marple method with extrapolation by a factor of 20 followed by Fourier processing

are shown in Figure 8(c). Clearly, for the higher SNR values considered in these calculations, the Marple method needs only 10 to 20% of the bandwidth required by conventional Fourier processing to achieve a resolution with a useful precision. For SNR values of only 20 dB, however, the Marple method is not as good as the Burg method.

Figure 9 summarizes these results by showing the BWE ratio limit versus SNR for the Burg and Marple methods. A value for the ratio limit at a specific SNR for either method was obtained as follows: the abscissa value of the SNR curve at the 0.2 precision level for the conventional method (Figure 8[a]) was compared to the corresponding value for that precision and SNR for the expansion method (Figure 8[b] or [c]). This limit is presented as an approximate bound for the expansion of a set of measured bandwidth data.

For an example of interpreting Figure 9, consider the case of a 35-dB SNR. If two scattering centers are separated by only one-half the distance corresponding to the resolution obtained by conventional Fourier processing, the Burg method will achieve a resolution with a 0.2 precision in the separation estimate. (Note that the ordinate of the Burg curve at 35 dB is greater than 2.) For the same SNR, if the two points are separated by only one-third the distance corresponding to the resolution obtained by conventional Fourier processing, the Burg method cannot provide the resolution but the Marple method can. (Note that the ordinate for the Marple curve at 35 dB is greater than 3.) When the BWE limit is satisfied, expansion beyond the limit will sharpen the resolved point responses.

Thus the crucial factor in choosing among the different BWE methods is the available SNR. Experience suggests that SNR values for field data are usually less than about 30 dB. Because the Burg method is robust, it is generally chosen for such data. But when the SNR is significantly higher than 30 dB, the Marple method can improve the resolution greatly.

Extended Coherent Processing

The development of the theory and methods for wide-angle imaging has been ongoing at Lincoln Laboratory since the early work by H.M. Jones for satellite targets in 1973 [12]. This theory has been described as correlation imaging, and the methods have been referred to as extended coherent processing (ECP). Related imaging theory in a slightly different signal coordinate set (radar frequency instead of slant range) was developed independently by J.L. Walker of the Environmental Research Institute of Michigan (ERIM) [13]; Walker's work uses a two-dimensional image processing that is frequently referred to as polar-format processing. (Note: These two imaging approaches were published jointly in 1984 [14].)

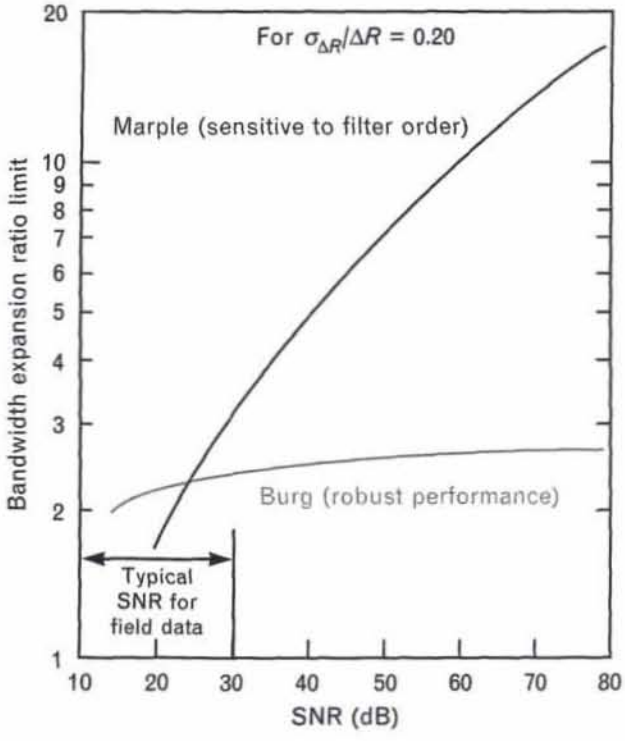

FIGURE 9. Comparison of enhanced-resolution limits for the Burg and Marple methods. For required BWE ratios below the curves, classical resolution is achieved and a higher expansion ratio will sharpen the resolved peaks. For required BWE ratios above the curves, resolution cannot be achieved.

As with more familiar optical imaging, radar image processing produces an intensity function that indicates the target configuration. In its idealized form, the processing produces a point-response function in two or three dimensions that peaks at the function's center and decays with distance away from the center in a manner dependent on the total angle and band-

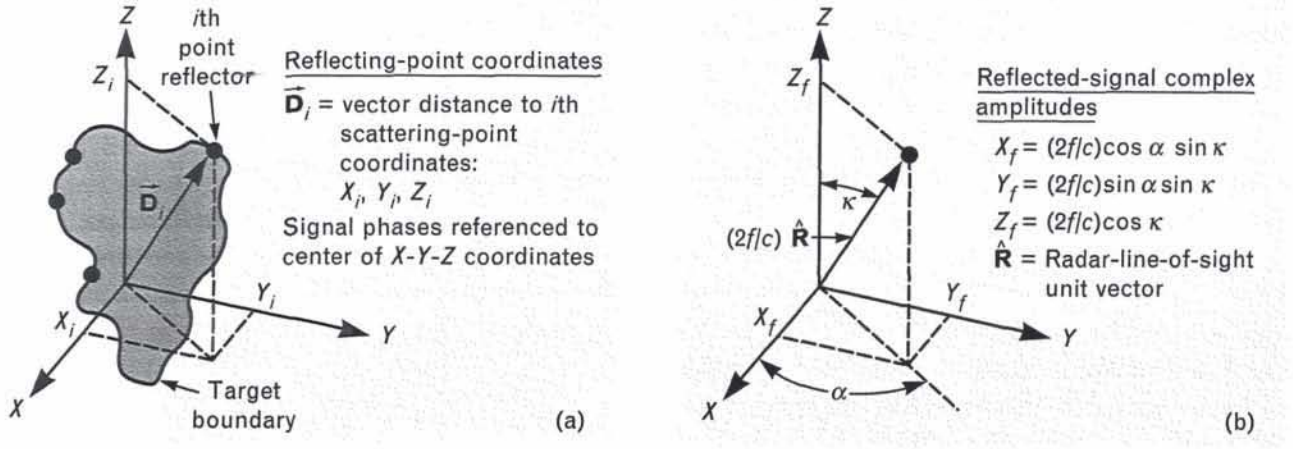

FIGURE 10. Coordinate systems for ECP theory: (a) target-fixed system and (b) signal-space definition. In the figures, f is the radar frequency and c is the speed of light.

width intervals of the integrated signal. This point response is replicated at each scattering-point location with a peak amplitude and phase factor that can differ between points. In practice, scattering will deviate from this discrete, isotropic point-reflection model, and image effects that can be caused by varying intensity with aspect, shadowing, specular surface phenomena, and multipath must be considered separately for different aspect conditions.

Figure 10(a) defines the model for an ideal point reflector in a target-fixed three-dimensional (3-D) coordinate system, and Figure 10(b) defines the signal-space coordinate system within which a unit direction vector $\hat{\mathbf{R}}$ for radar line of sight (RLOS) is shown. Signals are assumed to be collected for different radar frequencies in a band along each defined direction. Thus the signals can be viewed in a spherical-coordinate system of two angles and frequency that transforms to the rectangular-coordinate signal space shown in Figure 10(b). The reflected signal from the ith single point-scattering center is given by the equation

$$S_i = \sqrt{\sigma_i}\,\exp(j\phi_i),$$

where

$$\phi_i = -4\pi(f/c)\Delta R_i,$$

σ_i is the radar cross section of the ith point-scatterer, f is the radar frequency, c is the speed of light, and the relative slant range ΔR_i is given by the dot product between two vectors:

$$\Delta R_i = \hat{\mathbf{R}} \cdot \vec{\mathbf{D}}_i.$$

In terms of the rectangular signal-space coordinates, the general point response has the form of a 3-D sinusoid:

$$S_i = \sqrt{\sigma_i}\,\exp(j2\pi X_i X_f + j2\pi Y_i Y_f + j2\pi Z_i Z_f),$$

and the total signal from multiple points is

$$S_T = \sum_i S_i.$$

With the preceding condition, if rotations result in a distribution of RLOS aspects in both angles and frequency, the input signal may be viewed as a 3-D region in a volume bounded by bandwidth and the range of observed aspects. An appropriate integration that obtains an image intensity function in target coordinates is then a simple 3-D Fourier transform in the rectangular signal coordinates,

$$I(X,Y,Z) = \int_{X_f}\int_{Y_f}\int_{Z_f} S_T \cdot \exp\left[-j2\pi(XX_f + YY_f + ZZ_f)\right] dX_f\, dY_f\, dZ_f.$$

If the rotation axis is at a constant angle κ relative to the RLOS (sometimes called the aspect deviation angle) and $\kappa = 90°$, the signal region is in one plane and the image integral simplifies to a 2-D Fourier

transform. Furthermore, if the rotation rate is constant, the signals can be collected in polar form and interpolated for the rectangular form, and fast Fourier processing can then be applied to obtain an image. This procedure, which is sometimes called polar-format processing, has been used in other applications; its appeal comes from its computational simplicity. For the type of data and analyses described in this article, however, an alternative method (described below) has been more convenient for ECP.

An appropriate coordinate transformation allows the general 3-D image integral to be reformulated in spherical coordinates of angle and frequency. Within a small approximation, integration along the frequency axis for a fixed aspect becomes a Fourier transform that results in the amplitude-range sweep usually found in practical recordings. BWE processing expands this bandwidth, but the basic processing for ECP is not affected. The remaining integrations of the range-sweep data in angle coordinates cannot be represented by a 2-D Fourier transform.

For the constant $\kappa = 90°$ case, integration in only one angle is required, and it can be shown that a range-Doppler image is an approximation for this integral if the integration angles are small. Thus, as suggested by Jones, an approximate piecewise wide-angle integration can be effected by summing the responses from a set of range-Doppler images spanning the desired wide angle after the appropriate phase compensation and interpolation of the rotated-image grid data. A simplified illustration of this method was presented in Figure 3 for 20° rotation with examples of point-model responses. For sufficiently large rotation angles and for constant-amplitude scattering centers, range resolution is also improved. Integration computation efficiency is generally gained by performing fast Fourier processing for the range-Doppler imaging.

Even for a constant rotation rate, however, κ is generally not equal to 90°. Although the integration is with respect to one angle, the general imaging theory produces a 3-D distribution of responses. Approximate 2-D ECP images may be obtained that have less distortion than range-Doppler images and are treated in a similar geometric projection sense. Cuomo has developed another approach for 2-D imaging that uses *apparent* cross-range scaling of the range-Doppler images summed in an ECP set [15]. (In apparent cross-range scaling, the processing is performed as if $\kappa = 90°$; i.e., the apparent cross-range equals the true cross-range multiplied by $\sin\kappa$.) With these conditions, an apparent cross-range 2-D ECP image of an axisymmetric target can theoretically produce responses that indicate the true projection of the axisymmetric outline in a manner that can be useful for cases in which κ is large.

Examples of Super-Resolution

BWE Processing for Static Range Target Data

The following discussion presents individual range-sweep examples of BWE results based on static range measurement data. The results demonstrate the validity of the principles discussed earlier and they illustrate the effects that can be observed with well-defined targets that are not very complex. The Burg method was used to estimate the linear-prediction coefficients, and the steps in the processing were those presented in Figure 2. These steps included (1) transforming the input pulse data to the radar frequency domain; (2) removing the weighting function that had been used earlier for sidelobe reduction; (3) estimating the prediction coefficients; (4) keeping the original spectrum data and using the coefficients to obtain extrapolated data in both directions with the total extrapolated spectrum spanning a desired new bandwidth; and (5) transforming this extrapolated set with appropriate sidelobe-reduction weighting to obtain a new range-sweep response with finer range resolution.

The measurement data for two small spheres (Figure 2) are repeated in a slightly different form in Figure 11, with a complex-pair representation of the signal amplitudes in the radar frequency domain. The spheres were separated by approximately 4 in (10 cm) in slant range, the sphere diameters were 3/8 in (0.95 cm), and the center frequency of the transmitted band was 10 GHz. Figure 11(b) shows the 1-GHz-bandwidth segment of the original data and the extrapolated segments that were obtained with linear prediction. The extrapolations compare closely with the true 4-GHz patterns in Figure 11(a). The right-

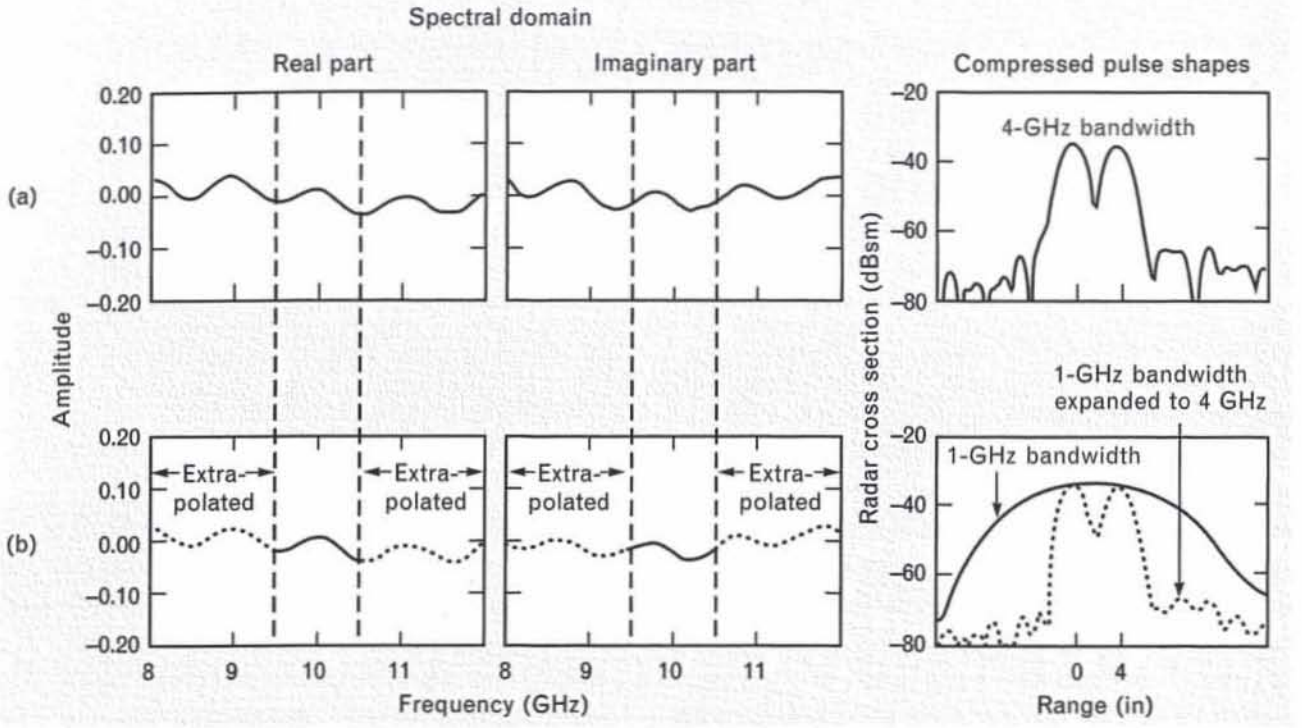

FIGURE 11. Data for two small spheres separated by 4 inches in slant range: (a) 4-GHz data and (b) BWE data showing the 1-GHz-bandwidth segment of the original data and the extrapolated segments that were obtained with linear prediction.

most plot of Figure 11(b) shows the two points unresolved in responses based only on 1-GHz data but resolved with the extrapolated data, and the latter pulse pattern compares well with the true 4-GHz pulse pattern shown in the right-most plot of Figure 11(a).

Figure 12 shows a series of radar pulse shapes obtained from an aluminum reentry vehicle (RV) model at a Lincoln Laboratory static radar range. Measurements were made every 10° in roll around the model's axis. In the figure, 37 pulse shapes for one entire roll period are stacked above one other. The transmitted and received signals are for linear polarization at X band. Figure 12(a) shows the original 2-GHz real bandwidth responses, Figure 12(b) shows the responses obtained with only the center 1-GHz real bandwidth, and Figure 12(c) shows the responses obtained for BWE extrapolation of the 1-GHz signals to 2 GHz. Note that the BWE responses compare well with the original 2-GHz responses.

The 2-GHz data and the results of extrapolation to a 6-GHz bandwidth are shown in Figure 13. From left to right, the first two returns in Figure 13(b) are from the nose and the junction between the nose and the conical afterbody of the RV model; note that these two returns are not resolved in Figure 13(a). The return from the base is observed in both plots and some of the returns following the base return are from the model support. In Figure 13(b), the third return, which occurred 27 cm behind the nose of the body, was not expected. Because these data were taken at linear polarization, this return was seen to be roll dependent. After careful inspection of the target, the source of the return became immediately obvious. The model had been constructed of sheet metal; Figure 14 contains two photographs of the model in which the blowup on the right shows both the seam and a rivet used to hold the sheet metal together. There were other rivets on the body, but they had tighter fits and, after being ground down, they were barely visible. The rivet that was 27 cm from the nose of the RV was not as well concealed and was the source of the third return in Figure 13(b).

Figure 15 shows static range wideband data mea-

sured on a conical vehicle. A very narrowband sampling from 2-GHz to 18-GHz center frequencies at steps of 20 MHz allowed representation of the wideband data at a variety of bandwidths at different center frequencies. In Figure 15, the pulse profiles for 1-GHz and 2-GHz bandwidths are shown at center frequencies from 4 to 16 GHz in 3-GHz steps. Clearly, 1-GHz resolution is not sufficient compared to the 2-GHz capability. The measured 1-GHz-bandwidth data were extrapolated by autoregression analysis techniques and presented in Figure 16 in comparison with the measured 2-GHz data. The figure shows excellent agreement between the BWE data and the measured data.

Simulated 2-D Super-Resolution Using Sequential 1-D Super-Resolution

Two-dimensional super-resolution was discussed briefly in the beginning of this article. In Figure 4, scattering from a conical vehicle with a height and base diameter of 1 and 0.5 m, respectively, was simulated with three point-scatterers. The simulation represented the scattered signal as a function of radar frequency and aspect angle, and was applicable to either ISAR or SAR interpretation. Figure 17 repeats the results shown in Figure 4 for the case in which the aspect deviation angle κ was 90°, and includes additional results for $\kappa = 75°$ and 60°. In an ISAR application, these examples represent a tumbling cone when the RLOS is in the tumble plane, 15° out of the tumble plane, and 30° out of the tumble plane (κ = 90°, 75°, and 60°, respectively). In a SAR application, the $\kappa = 75°$ and 60° cases represent lookdown angles of 15° and 30°, respectively.

The data were simulated for the equal-amplitude (0 dBsm) scattering centers at each aspect for radar frequencies from 1.035 GHz to 1.365 GHz in 10-MHz increments. Thus, from Equation 1, the signal bandwidth affords a classical range resolution of 82 cm. The aspect angles (between the cone axis and the RLOS projection on the plane of the scattering centers) are 23° to 37° with 1° increments. The classical cross-range resolution is given by $\lambda/(2\Delta\theta \sin\kappa)$, which results in 92, 95, and 106 cm for κ = 90°, 75°, and 60°, respectively. The pseudo-color images are shown for a 30-dB dynamic range, i.e., 10 3-dB contour increments.

The conventional images were created by first compressing the frequency data with Hamming weighting to obtain range profiles for each aspect angle. Then conventional angle (Doppler) processing with Hamming weighting was used to calculate the cross-range dimension. By contrast, the super-resolution image profiles were created by the following process:

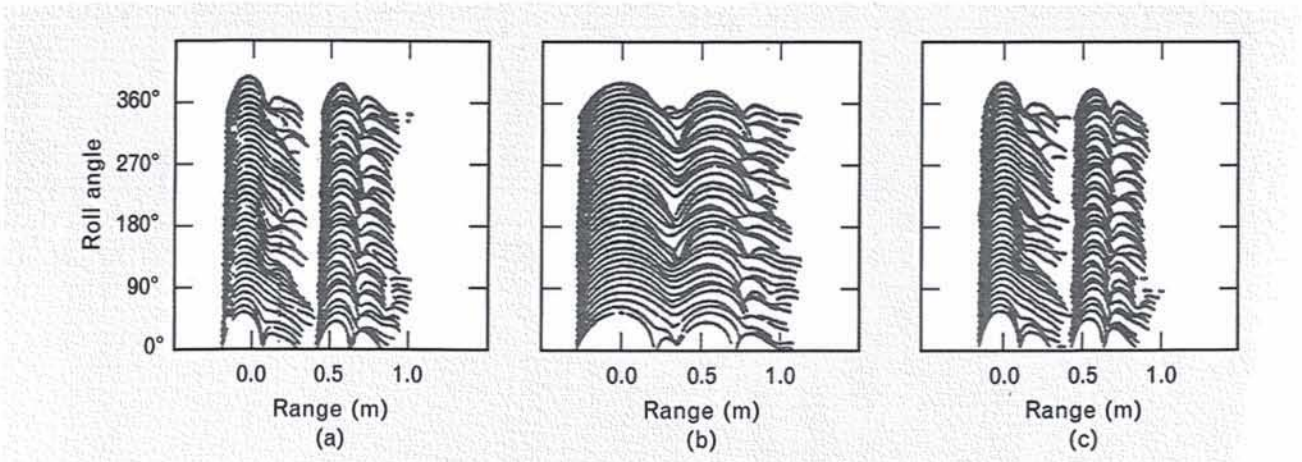

FIGURE 12. Series of radar pulse shapes: (a) original 2-GHz real bandwidth responses, (b) responses obtained with only the center 1-GHz real bandwidth, and (c) responses obtained for BWE extrapolation of the 1-GHz signals to 2 GHz. The data were obtained from an aluminum reentry vehicle (RV) model at a Lincoln Laboratory static radar range. Measurements were made every 10° in roll around the model's axis, and the transmitted and received signals are for linear polarization at X band. Note that the BWE responses compare well with the original 2-GHz responses.

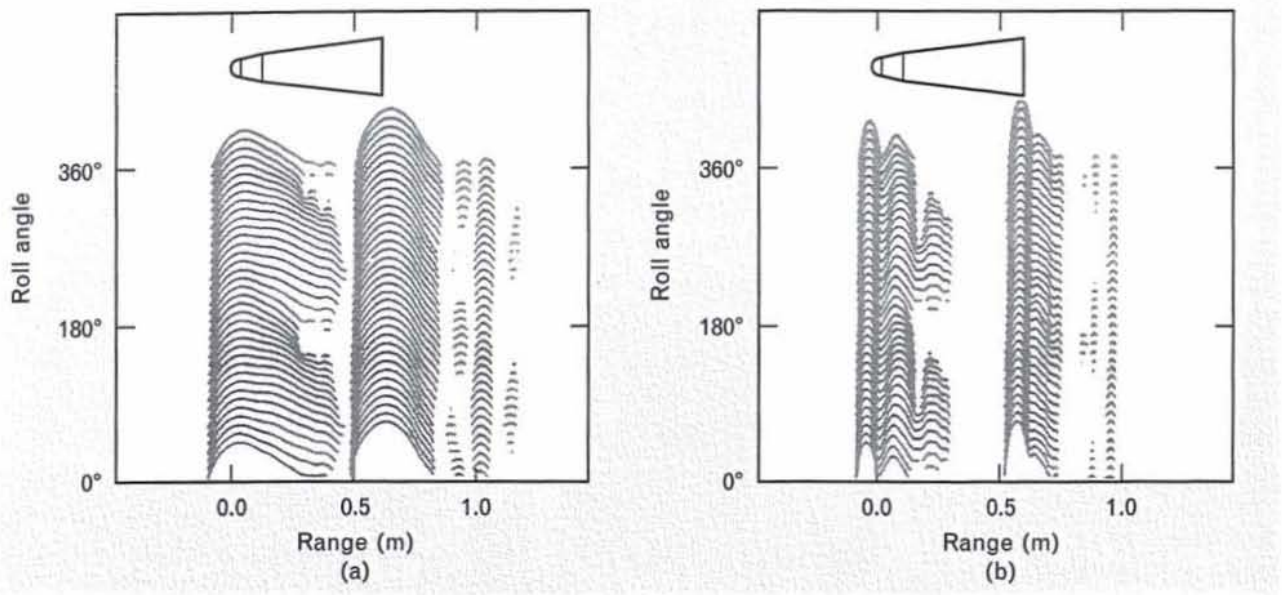

FIGURE 13. Series of radar pulse shapes: (a) original 2-GHz data and (b) 2-GHz data extrapolated to 6-GHz bandwidth. In part *b*, the first two returns (from left to right) are from the nose and the junction between the nose and the conical afterbody of the RV model; note that these two returns are not resolved in part *a*.

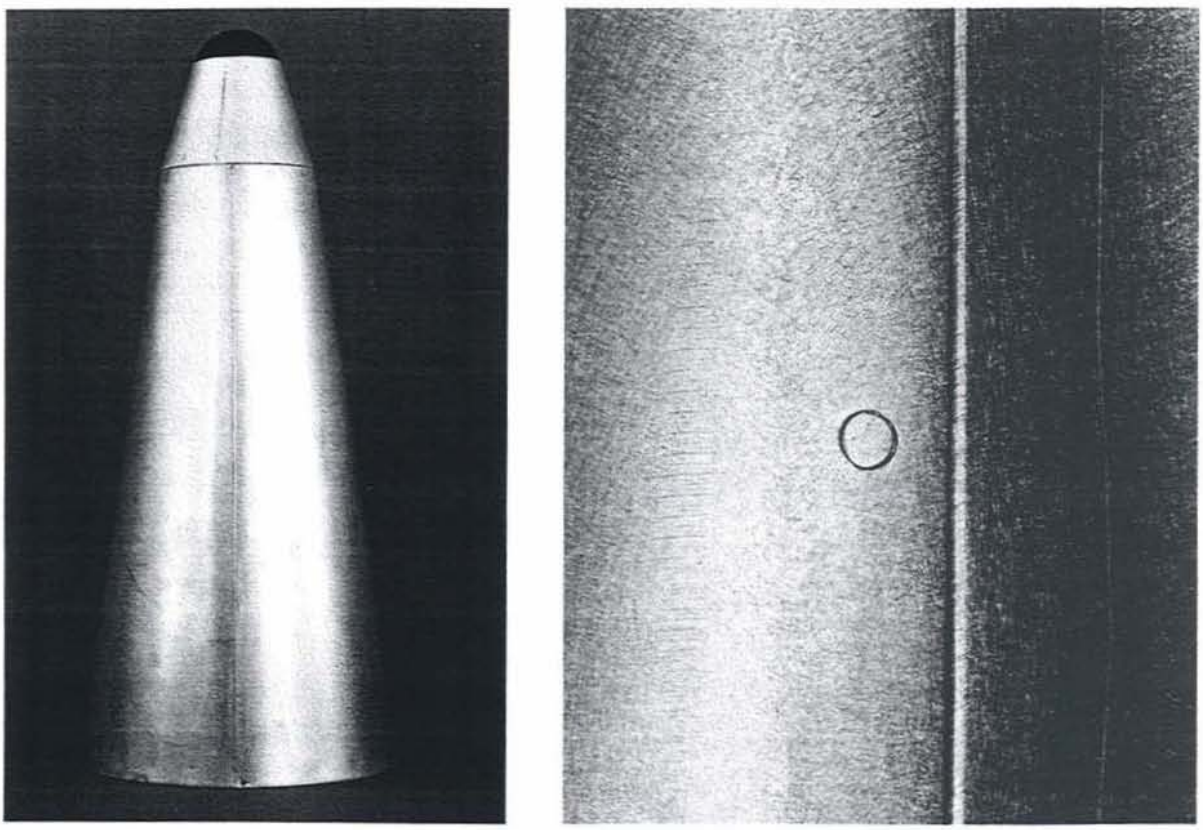

FIGURE 14. Photographs of target model used in Figures 12 and 13. The blowup on the right shows the rivet that was the source of the third return, which occurred 27 cm behind the nose of the body, in Figure 13(b).

(1) after conventional range profiles were obtained, angle data for each range gate were processed with the Burg algorithm to achieve linear expansion by a factor of 3; (2) conventional angle processing was then used to calculate the cross-range resolution; (3) at each cross-range gate, the range-profile data were transformed back to the frequency domain, the weighting was removed, and bandwidth extrapolation by a factor of 3 was obtained with the Burg algorithm; and, finally, (4) at each cross-range gate, the expanded frequency data were transformed back into the range-profile domain. As mentioned earlier, the sequential application of a one-dimensional algorithm can produce results that differ depending on the order of processing. The super-resolution images, however, indicate by comparison that the process significantly improves resolution.

The process results in improved range and cross-range resolution for one "linear" image, i.e., for a rotation angle $\Delta\theta$ that is constrained to allow no Doppler smearing in the image. If a complete rotation (360°) set of data is available, ECP methods can then be applied to the resulting set of linear images.

Summary and Conclusions

The examples of processed data from static range measurements and simulations presented in this article clearly demonstrate the significant practical value in improving the slant-range and cross-range resolution by modern spectral estimation methods. Table 1 presents a summary of these techniques and their benefits and limitations. Three important factors will affect the success of bandwidth extrapolation (BWE): (1) the conformity of the actual target reflectivity with the signal assumptions of the limited-number-of-points model, (2) the systematic errors that can distort signals relative to the model assumptions, including propagation effects, and, in particular, (3) the signal-to-noise ratio. Even under good conditions, the nonlinearity of the BWE processing can produce various distortions, such as low-level-signal suppression and spurious responses in wider-dynamic-range cases of multiple points, that would not be expected from real bandwidth data.

Among the methods considered for estimating the linear-prediction coefficients used in BWE, the Burg

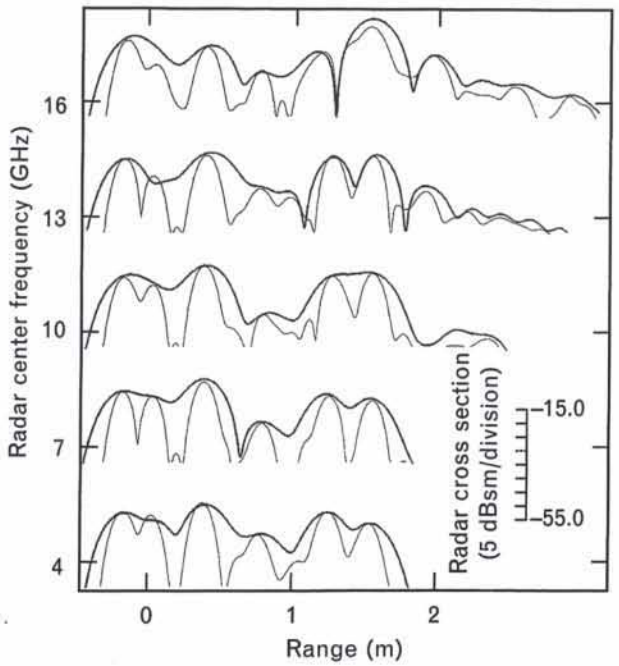

FIGURE 15. Static range wideband data measured on a conical vehicle for bandwidths of 1 GHz (red curves) and 2 GHz (blue curves) at different center frequencies. Note that the 1-GHz resolution is not sufficient compared to the 2-GHz capability.

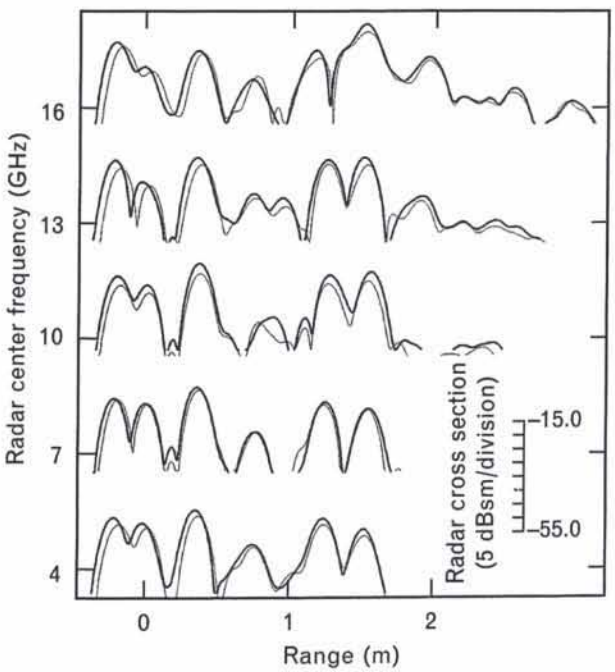

FIGURE 16. Static range data with BWE. The measured 1-GHz-bandwidth data of Figure 15 have been extrapolated by autoregression analysis techniques. Note the excellent agreement between the BWE data (black curves) and the measured 2-GHz-bandwidth data (blue curves).

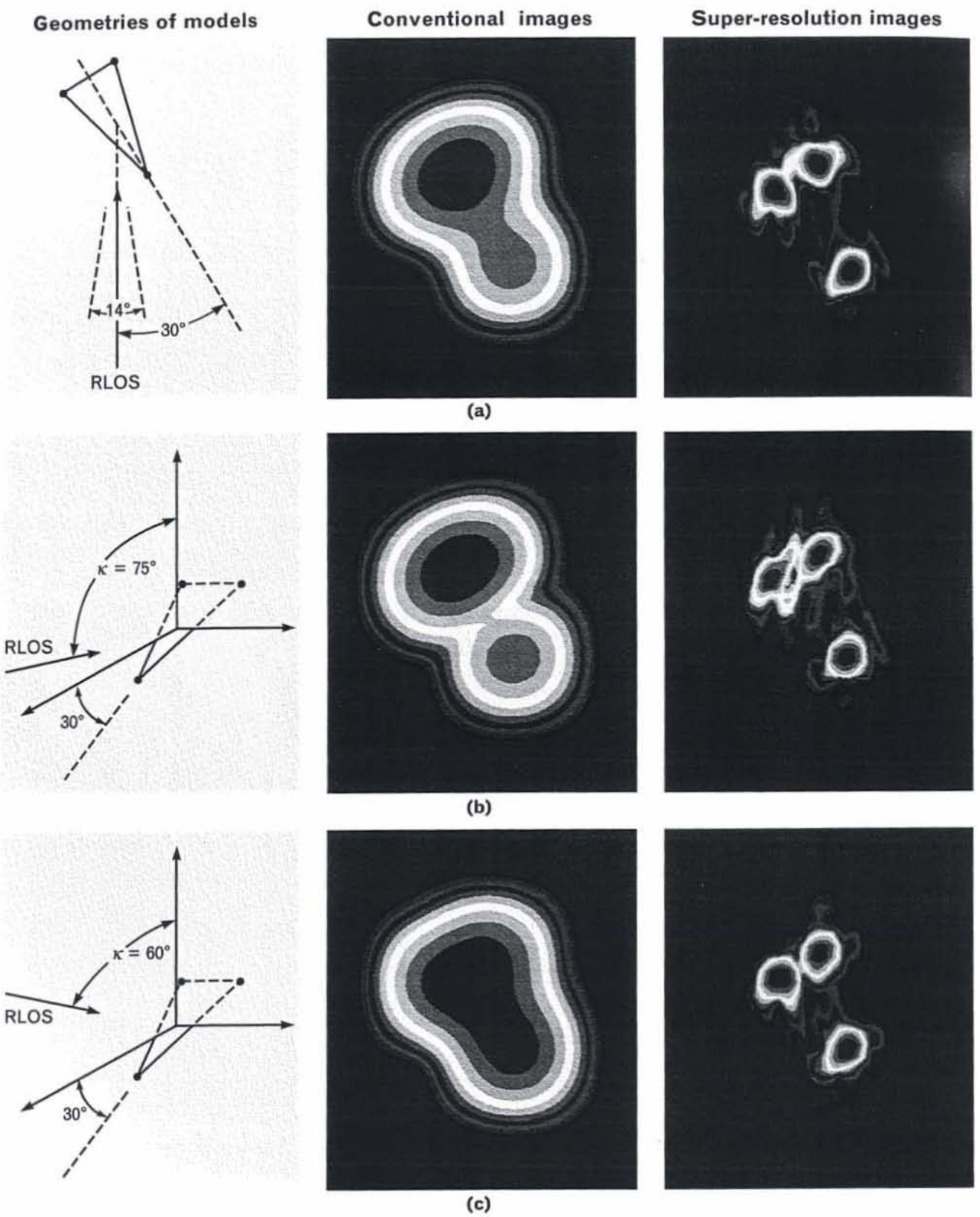

FIGURE 17. Conventional and super-resolution images for κ equal to (a) 90°, (b) 75°, and (c) 60°. The pseudo-color images are shown for a 30-dB dynamic range, i.e., 10 3-dB contour increments, and the horizontal and vertical directions are the cross-range and range, respectively.

Table 1. General Properties of Approaches to Spectral Analysis

	Conventional Fourier Techniques	*Autoregressive Models; Maximum Entropy*	*Combined Signal Extrapolation and Fourier Techniques*
Spectrum Concept	Fourier spectrum from projection of signal on sinusoidal basis functions.	Inverse squared magnitude of transfer function of whitening filter.	Fourier spectrum of data linearly predicted beyond original observation interval by using prediction coefficients.
Benefits	Linear operation conserves energy and preserves phase relationships. Has calibrated amplitude and phase spectra. Fast digital algorithms can be used.	Results in improved resolution of closely spaced spectral components.	Linearly extended data set maintains phase relationships and can improve resolution by at least a factor of 2. Regains resolution lost from use of weighting functions. Is suitable for vector and parallel processing for real-time applications.
Limitations	Places unrealistic constraints on the signal beyond the observation interval. Sidelobes and weighting functions limit detection and resolution.	Nonlinear process does not conserve energy. Has no phase information. Amplitudes are not calibrated. Occasional line splitting occurs.	Is not appropriate for a spectral continuum. Has larger computational load.

algorithm is generally practical because it guarantees the extrapolation will not result in exponential growth. This feature precludes catastrophic failure in any estimation attempt, and, in the limiting case of failure, it will tend to give at least the resolution of the original data. A constraint (Levinson) used in this method, however, limits the ability to resolve points spaced more closely together than the expanded bandwidth resolution if the expansion ratio is greater than approximately 3, even in the noise-free case. Greater BWE ratios can be used for purposes of further sharpening isolated responses in individual sweeps. This tactic is especially useful in wide-angle extended coherent processing (ECP).

Forward-and-backward linear prediction (FBLP) methods formulate least-squares residuals in a manner similar to that of the Burg algorithm, but they exclude the Levinson constraint. Marple has devised an efficient algorithm for this approach. The unconstrained FBLP estimation does not have the Burg limits of distortion effects in the two-point noiseless case, thus allowing a greater BWE ratio in some cases. Because exponential growth is possible, however, unstable extrapolations can result in the more general multiple-point case with noise. This instability can be controlled by limiting the coefficient numbers, but there then can be problems in too severe exponential damping. Tufts and Kumaresan have developed a method, based on the eigen-decomposition of matrices, for reducing the noise effects in the FBLP formulation for the linear least-squares estimates of coefficients. The method requires the point signal levels to be significantly higher than the noise levels, and does not appear attractive for situations in which the amplitudes cover a wide dynamic range.

The implications for future efforts are significant: (1) existing databases can be explored for applications to improve the derivable information, and (2) future radar system designs should include the ability to use modern spectral estimation

methods for improving resolution.

Acknowledgments

The authors express their sincere gratitude to the many individuals who contributed to this article. Principal contributors at Lincoln Laboratory include B. Sheeks, F.C. Wang, and E. Huang, and especially J. Brunner for developing estimates of improved range precision. In addition, A. Moceyunas, F. Piesel, and P. Jedrzejewski of the Syracuse Research Corp. have contributed significantly to the modeling, the precision estimates, and the detailed summaries of theoretical developments of bandwidth extrapolation and extended coherent processing.

This work was sponsored by the Army Space and Strategic Defense Command and the Air Force Foreign Aerospace Science and Technology Center.

REFERENCES

1. K.R. Roth, M.E. Austin, D.J. Frediani, G.H. Knittel, and A.V. Mrstik, "The Kiernan Reentry Measurements System on Kwajalein Atoll," *Linc. Lab. J.* **2**, 247 (1989).
2. A.L. Kachelmyer, "Range-Doppler Imaging with a Laser Radar," *Linc. Lab. J.* **3**, 87 (1990).
3. L.M. Novak, M.C. Burl, R.D. Chaney, and G.J. Owirka, "Optimal Processing of Polarimetric Synthetic-Aperture Radar Imagery," *Linc. Lab. J.* **3**, 273 (1990).
4. R.T. Lacoss, "Data Adaptive Spectral Analysis Methods," *Geophysics* **36**, 661 (1971).
5. J. Capon, "High-Resolution Frequency-Wavenumber Spectrum Analysis," *Proc. IEEE* **57**, 1408 (1969).
6. S.L. Marple, *Digital Spectral Analysis with Applications*, chaps. 12 and 16 (Prentice-Hall, Englewood Cliffs, NJ, 1987).
7. J.E. Evans, J.R. Johnson, and D.F. Sun, "Application of Advanced Signal Processing Techniques to Angle of Arrival Estimation in ATC Navigation and Surveillance Systems," *Technical Report 582*, MIT Lincoln Laboratory (23 June 1982), NTIS #AD-A118306/0.
8. S.B. Bowling, "Linear Prediction and Maximum Entropy Spectral Analysis for Radar Applications," *Project Report RMP-122*, MIT Lincoln Laboratory Radar Measurements Program (24 May 1977), DTIC #AD-A042817.
9. K.M. Cuomo, "A Bandwidth Extrapolation Technique for Improved Range Resolution of Coherent Radar Data," *Project Report CJP-60, Revision 1*, MIT Lincoln Laboratory (4 Dec. 1992).
10. R. Kumaresan, "Estimating the Parameters of Exponentially Damped or Undamped Sinusoidal Signals in Noise," Ph.D. dissertation, University of Rhode Island, Kingston, RI (Aug. 1982).
11. D.W. Tufts and R. Kumaresan, "Estimation of Frequencies of Multiple Sinusoids: Making Linear Prediction Perform like Maximum Likelihood," *Proc. IEEE* **70**, 975 (1982).
12. H.M. Jones and E.C. Poggio, private communications.
13. J.L. Walker, "Range-Doppler Imaging of Rotating Objects," *IEEE Trans. Aerosp. Electron. Syst.* **16**, 23 (1980).
14. D.A. Ausherman, A. Kozma, J.L. Walker, H.M. Jones, and E.C. Poggio, "Developments in Radar Imaging," *IEEE Trans. Aerosp. Electron. Syst.* **20**, 363 (1984).
15. K.M. Cuomo, private communications.

SIDNEY L. BORISON
is an associate leader of the Analysis Techniques and Interpretation Group. His focus of research has been on the acquisition and analysis of high-resolution radar data. In the 1960s he was active in the Lincoln Laboratory Wide Band Observables program, which led to the development of the ALCOR radar and wideband discrimination methods. Subsequently, he was instrumental in initiating Laboratory efforts in wideband-satellite-object-identification techniques, which included the methods of Inverse Synthetic-Aperture Radar (ISAR) applied to ALCOR data. He participated in the requirements definition and eventual analysis of data from the wideband Long Range Imaging Radar and the Firepond Laser Radar. For the last 10 years he has been principally involved with the application of these techniques to the analysis of wideband intelligence data collected from strategic missile targets. He received a B.S. and Ph.D. degree in physics from MIT.

STEPHEN B. BOWLING
is the leader of the Field Systems Group, which supports the instrumentation located at the Kwajalein Missile Range in the Marshall Islands. An additional responsibility is the direction of the Lexington Discrimination System (LDS), a testbed facility at Lincoln Laboratory for developing and validating real-time discrimination algorithms and logic for strategic and tactical missile defense systems. Since coming to Lincoln Laboratory in 1975, he has worked in a number of different areas spanning discrimination research, signal and data processing techniques, and sensor systems analysis. He received a B.S. degree in physics from the University of North Carolina at Chapel Hill, and an M.S. and a Ph.D. degree in space physics and astronomy from Rice University.

KEVIN M. CUOMO
is a staff member in the Analysis Techniques and Interpretation Group, where he specializes in the analysis of radar data collected by several systems, including COBRA JUDY, COBRA DANE, and the Kwajalein Missile Range radars. He has developed and implemented various radar imaging techniques, including extended coherent processing (ECP) to generate high-resolution three-dimensional radar images, and bandwidth extrapolation (BWE) to improve the range resolution of coherent radar returns. Before joining Lincoln Laboratory in 1988, he was a member of the research staff at Calspan Corporation.

Kevin received a B.S. (magna cum laude) and an M.S. degree in electrical engineering from the State University of New York at Buffalo in 1984 and 1986, respectively. A member of the Lincoln Laboratory Staff Associate Program, he is currently pursuing a Ph.D. degree in electrical engineering at MIT. For his thesis research, he has been investigating various signal processing and communications applications of nonlinear dynamic systems. He is a member of Tau Beta Pi, Eta Kappa Nu, and Sigma Xi.